EPTT 2024
Escola de Primavera de Transição e Turbulência

ABCM
Associação Brasileira de Engenharia e Ciências Mecânicas

EPTT-2024-0055
Analysis of dynamic stall for a simplified single blade vertical axis wind turbine configuration

Lucas Feitosa de Souza
Renato Fuzaro Miotto
William Roberto Wolf
School of Mechanical Engineering, University of Campinas, Campinas, SP, 13083-860, Brazil
l251480@dac.unicamp.br; miotto@fem.unicamp.br; wolf@fem.unicamp.br

Abstract. *The dynamic stall features of a simplified vertical axis wind turbine (VAWT) configuration are analyzed. Wall-resolved large eddy simulations (LES) are performed for a NACA0018 airfoil operating as a single blade VAWT, and the operational parameters are set to tip speed ratio $\lambda = 3$, Reynolds number $Re = 50,000$ and Mach number $M = 0.1$. The numerical model is validated by performing a grid convergence study as well as an analysis of the airfoil spanwise domain. Results suggest that a computational domain with 40% of the airfoil chord in the spanwise direction is sufficient to capture the underlying flow dynamics when compared with span lengths of 10% and 80% of the chord. A good agreement with literature results is observed in terms of the main flow features for similar setups both in terms of integral quantities and the overall flow behavior.*

Keywords: *LES, vertical axis wind turbine, dynamic stall, unsteady aerodynamics*

1. INTRODUCTION

Owing to their distinctive movement, VAWTS are susceptible to the effects of dynamic stall. This phenomenon occurs when the airfoil experiences variations in the angle of attack that surpass the static stall angle. The stall regime occurs for lifting surfaces undergoing transient motions, being characterized by significant fluctuations in aerodynamic loads, triggered by the sudden formation of a large vortex at the airfoil leading edge. These loads have the potential to couple with the structural dynamics of the turbine, posing a risk of mechanical failure (Corke and Thomas, 2015). For VAWTs, the initiation of the dynamic stall vortex occurs in the upwind segment of the movement and is associated with blades operating at low tip-speed ratios ($\lambda < 3$) (Laneville and Vittecoq, 1986; Simão Ferreira *et al.*, 2009; Fujisawa and Shibuya, 2001; Le Fouest and Mulleners, 2022). This dimensionless parameter is determined by the ratio between the airfoil and freestream velocities $\lambda = \omega R/U_\infty$, where ω is the angular velocity of the blade, R is the radius of the movement and U_∞ is the freestream velocity. This nondimensional parameter is linked to the amplitude and skewness of the variations in the effective inflow velocity and the blade angle of attack (Le Fouest and Mulleners, 2022).

Numerous experimental studies have delved into the effects of dynamic stall in the context of VAWTs (Laneville and Vittecoq, 1986; Fujisawa and Shibuya, 2001; Simão Ferreira *et al.*, 2009; Araya *et al.*, 2017; Le Fouest and Mulleners, 2022). For instance, Laneville and Vittecoq (1986) conducted experiments with a Darrieus turbine at an average Reynolds number of 3.8×10^4 and reported dynamic stall occurrences for tip-speed ratios less than 4. In a different study, Fujisawa and Shibuya (2001) utilized Particle Image Velocimetry (PIV) to examine the water flowfield over a small-scale Darrieus wind turbine. They observed two pairs of stall vortices during each turbine rotation cycle and attributed dynamic stall to the successive generation of flow separation over the inner surface of the blade. Additionally, Simão Ferreira *et al.* (2009) employed PIV to investigate the wind tunnel flow over a single-bladed NACA0015 airfoil in a Darrieus turbine configuration, operating with tip-speed ratios ranging from 2 to 4 and Reynolds numbers of 50,000 and 70,000. Focusing on the case with a tip-speed ratio of 2, they noted that, for both Reynolds numbers, no discernible differences in flow behavior were evident. This was attributed to the dominance of the dynamic stall process by laminar separation at the leading edge.

Araya *et al.* (2017) explored the wake generated by different configurations of vertical axis wind turbines with varying numbers of blades. Their findings revealed that the far wake exhibited features quantitatively similar to bluff body wakes, particularly for similar aspect ratios. More recently, Le Fouest and Mulleners (2022) utilized PIV to analyze the correlation between dynamic stall and the aerodynamic performance of a single-bladed H-type Darrieus wind turbine. Their results indicated that a peak tangential force is attained at low tip speed ratios ($\lambda < 2.5$). However, the formation of a large

dynamic stall vortex in the post-stall portion of the movement led to a substantial increase in drag, causing significant load variations that could compromise the structural integrity of the blade. The study also highlighted that, at intermediate tip-speed ratios ($2.5 < \lambda < 4$), there is a favorable compromise between increased tangential force and load variations, making this range the ideal operational zone for such devices.

Dynamic stall has also been a subject of investigation using Computational Fluid Dynamics (CFD) techniques, particularly for different types of airfoil motion (Lui and Wolf, 2019; Miotto *et al.*, 2022a, 2021; Ramos *et al.*, 2019a; Benton and Visbal, 2019; Batther and Lee, 2022). However, the cyclic motion characteristic of VAWTs poses unique challenges to numerical simulations, prompting a recent surge in studies exploring the dynamic stall phenomenon through CFD (Simão Ferreira *et al.*, 2010; Firdaus *et al.*, 2015; Liu *et al.*, 2022; Franchina *et al.*, 2022; Aboelezz *et al.*, 2022; Hao *et al.*, 2022; Venkatraman *et al.*; Ahnn and Choi, 2023). For instance, Simão Ferreira *et al.* (2010) investigated dynamic stall in a 2D NACA0015 VAWT, employing different modeling techniques and comparing their results with experimental data obtained through PIV. Firdaus *et al.* (2015) conducted 2D numerical simulations of a NACA0018 vertical axis wind turbine, utilizing the unsteady Reynolds-averaged Navier-Stokes (uRANS) equations with various turbulence models. More recent studies, such as Liu *et al.* (2022), explored the impact of suction and blowing actuation on the aerodynamic and aeroacoustic performance of Darrieus type-H wind turbines using 2D and 3D hybrid RANS-LES models. They reported optimal positional combinations for the actuator that led to improvements in aerodynamic coefficients and noise reduction. Additionally, Franchina *et al.* (2022) simulated the flow around a Tropskein vertical axis wind turbine using the uRANS equations with the k-ω SST turbulence model. Other investigations include Aboelezz *et al.* (2022), who utilized a uRANS approach to study the effects of passive flow control with a guided vane on a Darrieus wind turbine. Similarly, Hao *et al.* (2022) conducted RANS simulations with a transitional SST turbulence model to analyze the effects of deformable trailing edge flaps on a VAWT with a NACA0015 airfoil, focusing on load reduction and aerodynamic improvement. Further advancements include the work by Venkatraman *et al.*, who performed LES for a three-dimensional setup of a VAWT to investigate noise radiation using a Lattice-Boltzmann approach. The results showed good agreement with experimental data, particularly in terms of tonal peaks at the blade passing frequency and broadband levels. Lastly, Ahnn and Choi (2023) conducted LES using the incompressible Navier-Stokes equations to analyze the aerodynamic performance of different VAWT configurations operating in distinct flow regimes.

In reviewing the current state-of-the-art research on dynamic stall in the context of VAWTs, certain gaps in the literature are apparent, creating an opportunity for the present study to contribute with valuable insights. Several numerical investigations employ a RANS approach with turbulence models, limiting the extraction of detailed information about boundary layer phenomena. This includes understanding the mechanisms triggering the onset of the leading-edge vortex and the transient events governing the physics of dynamic stall. Even experimental studies face challenges in analyzing these aspects due to limited spatial resolution near the airfoil surface. To address these gaps, the current work endeavors to provide in-depth insights into these phenomena through high-fidelity numerical simulations. Here, we present a study focused on validating a model using a NACA0018 airfoil operating as a single-bladed VAWT. Simulations are performed for conditions with tip speed ratio $\lambda = 3$ and Reynolds number $Re = 5 \times 10^4$. These flow and kinematic parameters are based on the work from Le Fouest and Mulleners (2022), and are associated to induce a light stall regime. The model validation encompasses a grid convergence study and an exploration of the effects of domain size. Computational domains of 10%, 40%, and 80% of the chord in the spanwise direction are considered, shedding light on the requirements of this parameter for the accuracy of the simulations and for capturing important flow features.

2. Theoretical and numerical methodology

Wall-resolved LES are performed on a single NACA0018 airfoil under the characteristic motion of VAWTs by solving the compressible form of the Navier-Stokes equations. An O-type grid is employed and, therefore, the equations are solved in a general curvilinear coordinate system. The spatial discretization of the flow equations is performed using the sixth-order accurate compact finite-difference scheme from Nagarajan *et al.* Nagarajan *et al.* (2003). This methodology solves the advective and viscous fluxes using a staggered grid setup. The sixth-order compact interpolation scheme presented in the previous reference is also employed to interpolate flow quantities in the staggered grid approach.

The equations are solved in nondimensional form and in a non-inertial frame of reference. The characteristic length, velocity components, density, pressure, and temperature are given, respectively, by the airfoil chord c, freestream speed of sound a_∞, freestream density ρ_∞, $\rho_\infty a_\infty^2$, and $(\gamma - 1)T_\infty$. Here, T_∞ is the freestream temperature and γ is the ratio of specific heats. The motion effects are accounted for by reevaluating the right hand side of the momentum and total energy equations at every timestep. This approach entails no overhead, as the mesh can be kept fixed for any displacements of the airfoil.

The time integration of the flow equations is performed using an explicit third-order compact-storage Runge-Kutta scheme in regions away from solid boundaries. Near the airfoil surface, an implicit second-order scheme is applied to overcome the stiffness problem typical of boundary layer grids. Sponge layers and characteristic boundary conditions based on Riemann invariants are applied in the farfield, and adiabatic no-slip boundary conditions are used at the airfoil surfaces. The present numerical tool has been validated against experimental results and high-fidelity numerical simu-

lations of turbulent flows (Nagarajan *et al.*, 2003; Bhaskaran and Lele, 2010; Wolf *et al.*, 2012), besides the study of dynamic stall (Ramos *et al.*, 2019b; Miotto *et al.*, 2022b, 2021).

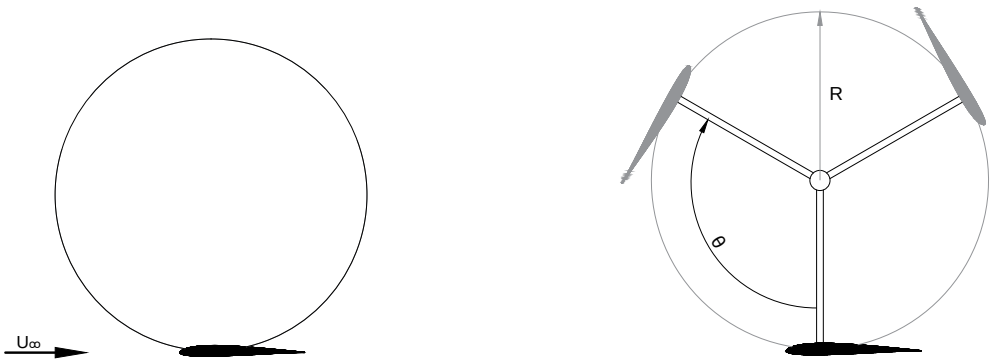

Figure 1. Schematic representation of the single bladed VAWT simulated (left) and the geometrical parameters θ and R used as reference to the position of the blade (right).

A shematic image of the setup used in the present simulations is shown in Fig. 1. The simulations are performed with the airfoil motion beginning at the topmost position, but the first half cycle is discarded due to initial transients, and the results are reported with the starting point being the bottommost position. A mesh refinement investigation is conducted to ensure the credibility of the presented results. The information regarding the meshes employed can be found in table 1 where nx refers to the number of points used to discretize the airfoil surface, ny is the number of points in the normal direction to the surface and nz is the number of points in the spanwise direction. Four simulations are conducted for the current investigation considering domain sizes in the spanwise direction corresponding to 10%, 40% and 80% of the airfoil chord.

Grid	span	nx	ny	nz	Total
1	0.1	640	450	24	6.91 M
2	0.4	640	450	80	23.04 M
3	0.4	720	540	104	40.43 M
4	0.8	720	540	208	80.87 M

Table 1. Description of the grids employed in the current investigation

In all our simulations, we maintain a constant Reynolds number of $\mathrm{Re}_c = 5 \times 10^4$ and a tip speed ratio $\lambda = 3$. For the investigation of grid refinement and the assessment of spanwise domain effects, we have selected a Mach number of 0.1. We made this choice due to the fact that we are solving the compressible form of the Navier-Stokes equations and, therefore, lower Mach numbers can lead to excessively extended integration times due to time step constraint. However, it is important to note that there is a substantial variation in relative velocity for the blades throughout the cycle, creating flow conditions that are not commonly encountered in the operation of a VAWT, due to compressibility effects. Nonetheless, this choice does not preclude the use of the collected data to validate the model.

3. Results

3.1 Grid refinement study

To assess the effect of mesh refinement and ensure that the results obtained are invariant with respect to this aspect, simulations are performed with grids 2 and 3 of table 1. The spans are the same, but the number of grid points is increased from grid 2 to 3. In this context, the resolution is improved in the streamwise direction of grid 3. Moreover, an additional clustering of grid points is also applied in the wall-normal direction through a smooth stretching, and the resolution is also enhanced along the spanwise direction. The analysis using integral quantities provided by Fig. 2 clearly demonstrates the independence of the results obtained, especially in the initial stages of each cycle, in which the dynamic stall vortex is formed. This initial stage is the most important in the present work, as it contains the physical mechanism of unsteady boundary layer separation. During the TEV detachment regime, small discrepancies are observed in the aerodynamic

coefficients, most evident in the moment coefficient. However, this is an expected effect as this stage of the flow is especially susceptible to cycle-to-cycle variations (Visbal, 2011).

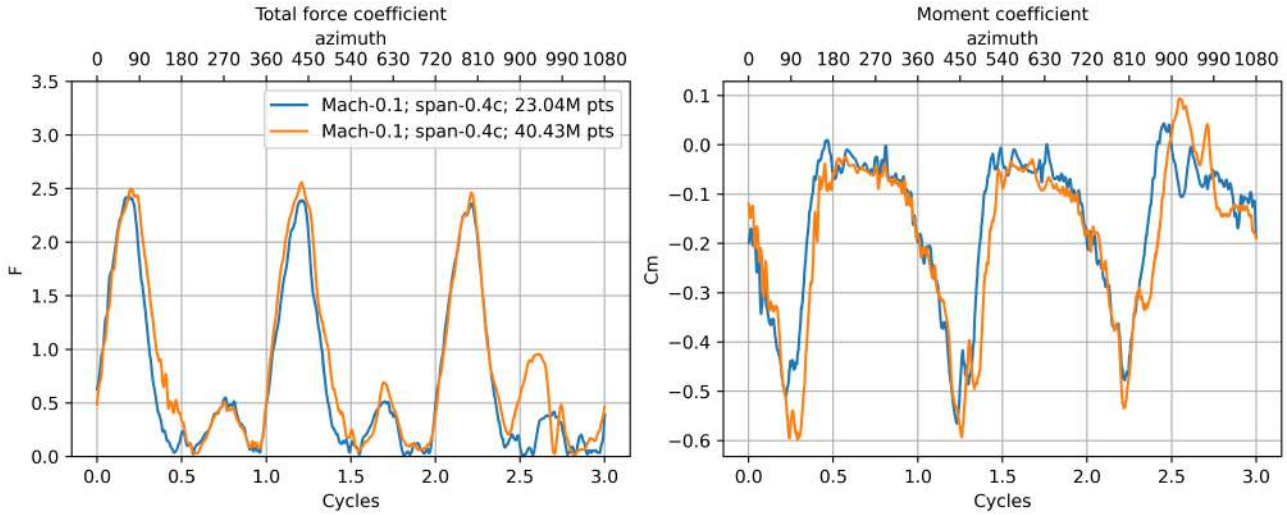

Figure 2. Total force (left) and pitching moment coefficient (right) for 3 cycles of the VAWT motion. The quantities are compared for simulations performed with grids 2 and 3 from table 1.

3.2 Main flow features

Figure 3 present snapshots for an airfoil with a span of $0.4c$. The images show the flow over the airfoil at four distinct azimuthal positions throughout the turbine cycle, in which the variations in the effective angle of attack induce dynamic stall. Starting with Figure 3 (a), the turbine is positioned at $\theta = 0$, directly facing the freestream. At this stage, a laminar boundary layer predominantly covers most of the airfoil, with only a small section near the trailing edge transitioning into turbulence. During the motion from Figs. 3 (a) and (b), the airfoil surpasses the static stall angle. This prompts instabilities in the shear layer, causing the transition point to move upstream along the airfoil chord. This process gives rise to a turbulent boundary layer and the accumulation of negative vorticity into a Turbulent Separation Vortex (TSV) in a process similar to what is shown in Benton and Visbal (2020) for a NACA0012 airfoil moving with a constant rate ramp-type pitch motion at the same Mach number. In our simulations, the TSV forms further downstream, as a thicker airfoil is more prone to trailing edge stall (McCroskey, 1981).

Between the snapshots from Figs. 3 (b) and (c), the TSV induces a shift in the flow circulation near the trailing edge, leading to the formation of a trailing edge vortex (TEV) with positive vorticity. This latter structure causes the TSV to detach from the surface of the airfoil reducing the overall force on the airfoil trailing edge which, in turn, leads to a reduction in the magnitude of the moment coefficient, as can be observed in Fig. 2. These phenomena subject the airfoil to larger forces than those experienced in static stall conditions and this behavior is well-documented in the literature for various types of motion and flow conditions (McCroskey, 1981; Le Fouest and Mulleners, 2022). It is important to point out that, for the motion comprehended between stages (a) and (b) of the figure, some qualitative divergences are observed compared to experimental results at the same tip speed ratio (for an incompressible flow) (Le Fouest and Mulleners, 2022). In the experiments, a light stall condition occurs including a small region of separated flow over the airfoil surface. In this regard, for our simulations the region of the separated flow becomes considerably larger than those reported in the literature. This disparity may be due to the fact that, during this stage, at the current Mach number, the flow almost reaches sonic speeds in the airfoil suction side leading to important compressibility effects that are not present in the previous experimental investigations. Moreover, the experiments may also have three-dimensional effects introduced by endplates and domain confinement that are not present in the simulations.

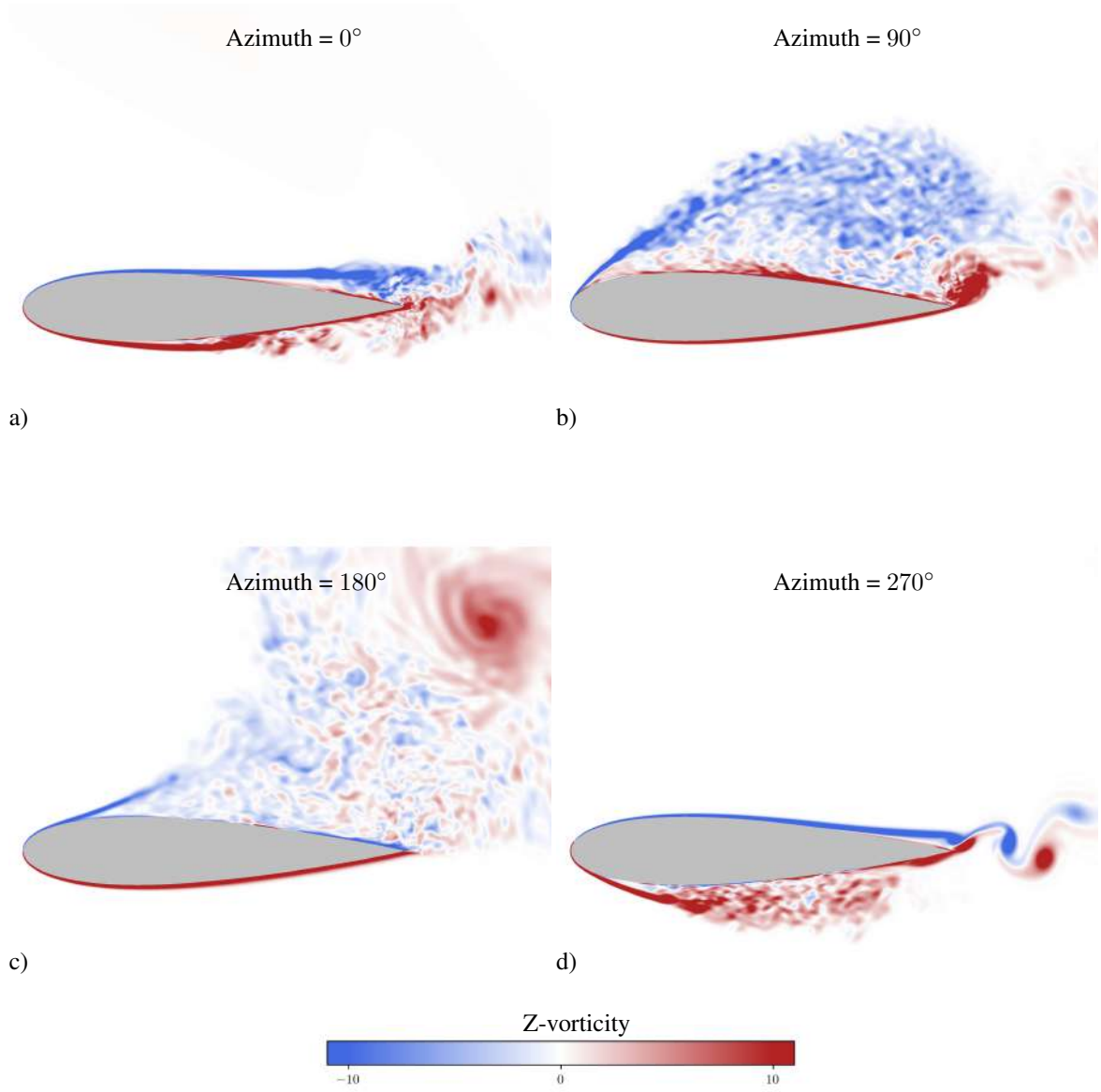

Figure 3. Z-vorticity contours for different stages of the cycle of a VAWT. Flow comes from left to right and the instants represent: a) attached flow; b) accumulation of vorticity and formation of a turbulent separation vortex; c) separated flow and emergence of the trailing edge vortex; d) relaminarization of the boundary layer.

The role of compressibility in the dynamics of the flow in this type of motion has not been catalogued in the literature yet, but for different types of motion it was found that increased compressibility can even lead to changes in the type of separation mechanism (Carr and Chandrasekhara, 1996). Although different from the incompressible regime, the results reported here are qualitatively similar to the numerical results reported by Visbal for a periodic pitching airfoil under light stall conditions at the same Mach number. Then, the larger length of the separation zone observed here is attributed to compressibility effects near the trailing edge of the airfoil which induces a stronger TEV. It is also worth pointing out that this latter structure is not observed in experimental results due to spanwise end-wall effects which can introduce three-dimensional effects in the flow, specially in the formation stages of the TEV for low aspect ratio wings (Garmann and Visbal, 2018).

Lastly, between the stages represented in Figs. 3 (c) and (d), the large coherent structures formed in the previous stages are transported, and the flow transitions back to a laminar state on the upper surface of the airfoil. At the lower surface, in turn, the static angle of attack is surpassed inducing separation and accumulation of positive (counterclockwise) vorticity. However, the asymmetric nature of the flow leads to a higher local pitch rate for the last portion of the movement yielding a weaker counterclockwise vortex in agreement with experimental observations (Henne *et al.*, 2020; Le Fouest and Mulleners, 2022). At this stage, the local Mach number is far inferior to that observed during the upstroke, reducing

the compressibility effects. As a result, the flow behavior is more similar to that observed for incompressible regimes. This observation supports our hypothesis that, additionally to the endwall effects introduced by experimental setups, the qualitative divergence during the upstroke is also enhanced by the high compressibility experienced by the flow during the upwind portion of the blade movement, due to the increased relative velocity.

3.3 Spanwise domain effects

In the present simulations, periodic boundary conditions are assumed in the spanwise direction. Therefore, the wavenumber of instabilities that may arise in this direction is limited by the size of the domain considered. So, it is also important to assess the effect of this variable on the flow dynamics. For this purpose, simulations are conducted considering domains equivalent to 10, 40 and 80% of the chord in the spanwise direction. For comparison, Fig. 4 presents snapshots obtained with the computational domains considered in the present investigation.

The impact of this parameter in the instantaneous characteristics of the flowfield is depicted in Figs. 5 and 6 for the second and third cycles of the movement. These figures depict the evolution of the vorticity field calculated through spanwise averaged solutions at three different instants during the upwind part of the movement. Each line corresponds to the instantaneous vorticity field at the corresponding azimuthal positions 72º, 108º and 144º, and each column divides the results obtained with the three different domain sizes for sake of comparison. Integral quantities are also shown in Fig. 7, which depicts the evolution of the total force coefficient (left) and moment coefficient (right) that the blade is subjected at each stage of the movement for the three cycles.

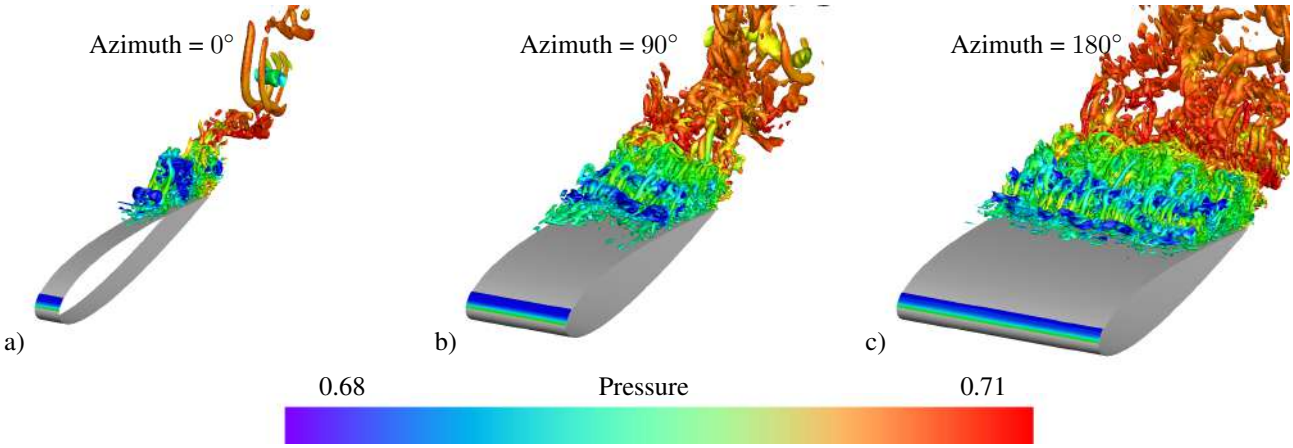

Figure 4. From left to right, the images show the computational domains that have 10% (a), 40% (b) and 80% (c) of the chord in the spanwise direction.

Comparing the instantaneous vorticity field for the same positions of the cycle, it is clear that the simulation with the computational domain limited to 10% of the airfoil chord presents well defined two-dimensional structures, especially during the upwind part of the blade motion, when we have the onset of dynamic stall. The interaction of these two-dimensional highly energetic structures in the case with a smaller domain results in a greater cycle-to-cycle variation in the aerodynamic coefficients. The cases with larger computational domains, in turn, depict a better comparison with respect to the integral quantities, since the vortex structures are subject to a turbulent regime, being broken into smaller and more uncorrelated scales, whose dynamics have less potential of influence over the aerodynamic forces and vortex interactions.

Comparing the case for the azimuthal position of 72º, especially, one can see structures generated by a Kelvin-Helmholtz instability that are still well defined in the case with a smaller computational domain, while in the cases with larger domains, the transition process to turbulence seems to happen in a more abrupt fashion. This fact directly impacts the coalescence process that gives rise to a dynamic stall vortex in the following moments for the smallest domain. This is evident for the position of 144º, which presents well-defined vortices shed from the leading edge (in blue color) for the case with the smallest spanwise domain, while for the larger domains, one can only see a thick region of uncorrelated separated flow with negative vorticity. Moreover, the simulation performed with the smallest domain also diverges from the others with respect to the moment when the TEV emerges, as can be seen by comparing the contours at the azimuthal position of 108º for both cycles. Computations considering spanwise domains of 0.4c and 0.8c present good agreement in terms of the flow features at each stage of the cycle (especially for the third cycle) and for the integral properties evaluated. The results presented in this section alongside the results from the grid refinement study suggest that mesh 2 with a spanwise domain size of 0.4 chord would be sufficient to accurately characterize the dynamic stall phenomenon for this flow configuration.

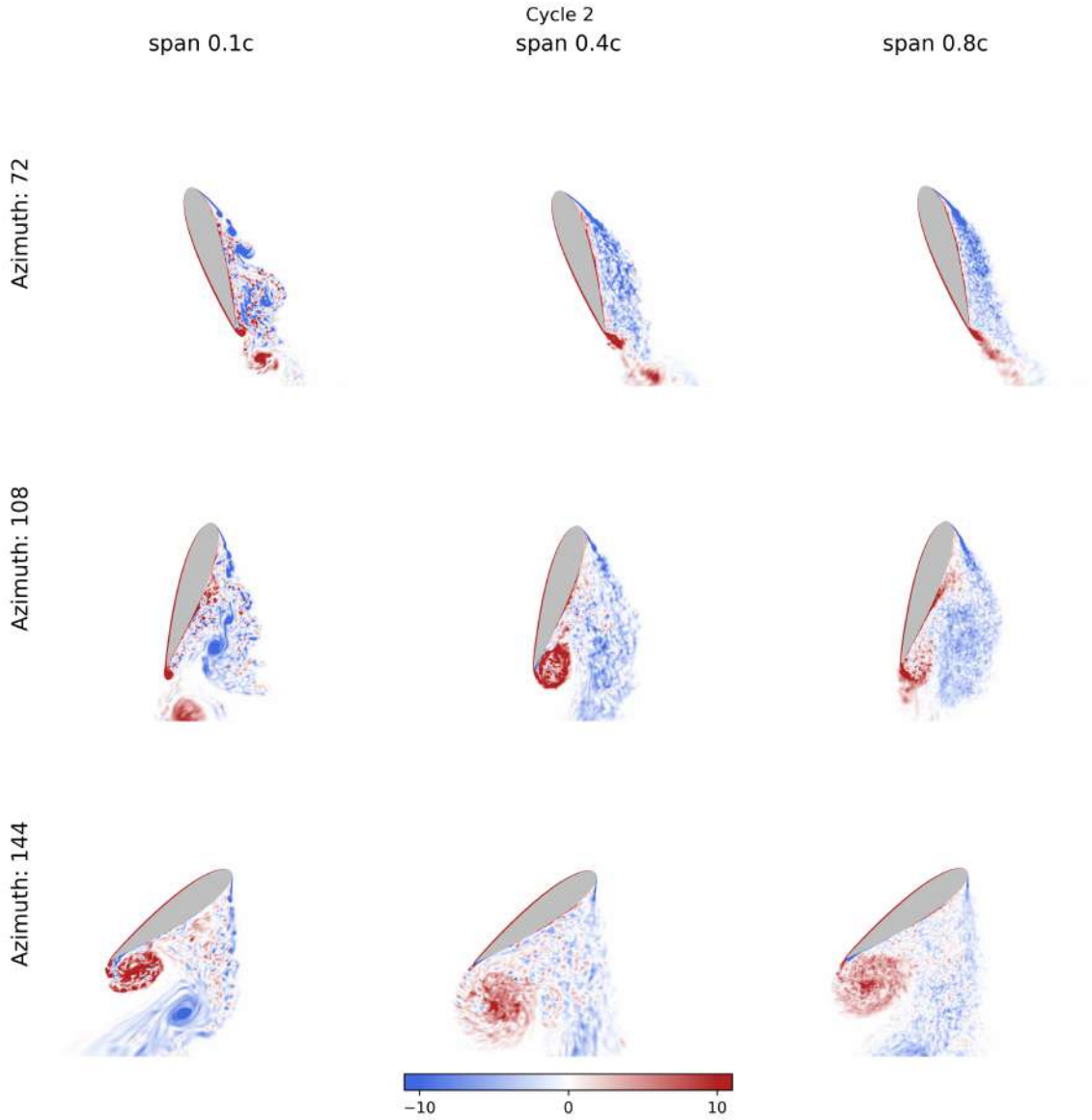

Figure 5. Spanwise-averaged vorticity contours computed for cycle 2 of the VAWT motion with grids 1, 3 and 4 from table 1. The different rows present snapshots for different airfoil positions in the VAWT motion and the different columns show results obtained for different spanwise domain sizes.

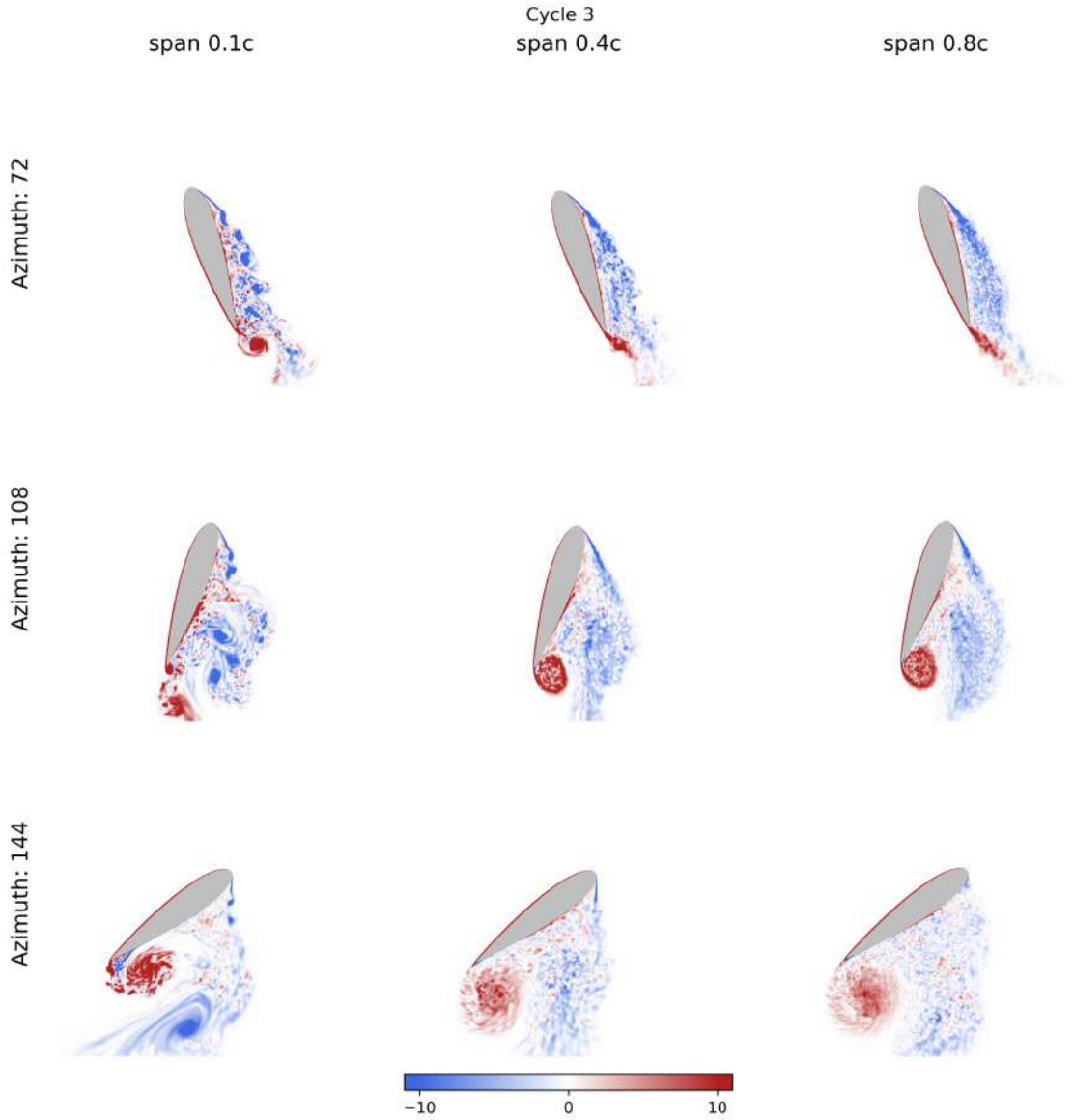

Figure 6. Spanwise-averaged vorticity contours computed for cycle 3 of the VAWT motion with grids 1, 3 and 4 from table 1. The different rows present snapshots for different airfoil positions in the VAWT motion and the different columns show results obtained for different spanwise domain sizes.

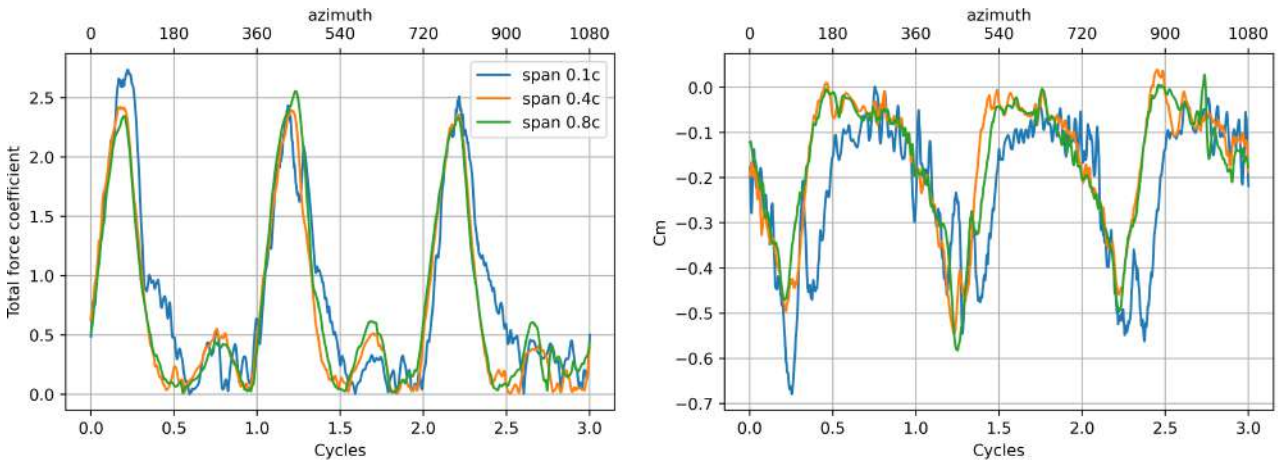

Figure 7. Total force (left) and pitching moment coefficient (right) for 3 cycles of the VAWT motion. The quantities are compared for simulations performed with grids 1, 3 and 4 from table 1.

4. Conclusions

We perform wall-resolved LES of a NACA0018 airfoil operating as a single-bladed VAWT. The simulations capture the the features of the dynamic stall phenomenon and show good agreement with the main trends reported in literature for a similar flow setup. The model employed is validated by a grid convergence study followed by an investigation of the effects of different sizes of computational domain in the spanwise direction. The results demonstrate good agreement in terms of integral properties and the overall flow features, especially during the upwind portion of the movement, where the dynamic stall onset occurs. Comparison between different configurations suggests that a computational domain of 40% of the airfoil chord is sufficient to capture the main flow dynamics. Qualitative differences with experimental data reported in the literature are attributed to compressibility effects present in the current simulated conditions and also to endwall and confinement effects from experimental setups.

Acknowledgments

The authors acknowledge Fundação de Amparo à Pesquisa do Estado de São Paulo, FAPESP, for supporting the present work under research grants No. 2013/08293-7, 2013/07375-0 and 2021/06448-0. FAPESP is also acknowledged for the scholarships provided to the first and second authors under grants No. 2022/08567-9 and 2022/09196-4, respectively. The CEPID-CeMEAI cluster Euler, CENAPAD cluster Ada Lovelace, and cluster SDumont are acknowledged for providing the computational resources for this research.

5. REFERENCES

Aboelezz, A., Ghali, H., Elbayomi, G. and Madboli, M., 2022. "A novel vawt passive flow control numerical and experimental investigations: Guided vane airfoil wind turbine". *Ocean Engineering*, Vol. 257, p. 111704.

Ahnn, S.nd Choi, H. 2023. "Leading-edge vortex and aerodynamic performance scaling in a simplified vertical-axis wind turbine". *Physics of Fluids*, Vol. 35, No. 10, p. 105140. ISSN 1070-6631. doi:10.1063/5.0166161. URL https://doi.org/10.1063/5.0166161.

Araya, D.B., Colonius, T. and Dabiri, J.O., 2017. "Transition to bluff-body dynamics in the wake of vertical-axis wind turbines". *Journal of Fluid Mechanics*, Vol. 813, p. 346–381. doi:10.1017/jfm.2016.862.

Batther, J. and Lee, S., 2022. "Numerical investigation of a pitching airfoil undergoing dynamic stall using delayed detached eddy simulations". *Computers & Fluids*, p. 105691.

Benton, S. and Visbal, M., 2019. "The onset of dynamic stall at a high, transitional reynolds number". *Journal of Fluid Mechanics*, Vol. 861, pp. 860–885.

Benton, S.I. and Visbal, M.R., 2020. "Effects of compressibility on dynamic-stall onset using large-eddy simulation". *AIAA Journal*, Vol. 58, No. 3, pp. 1194–1205. doi:10.2514/1.J058681. URL https://doi.org/10.2514/1.J058681.

Bhaskaran, R. and Lele, S.K., 2010. "Large eddy simulation of free-stream turbulence effects on heat transfer to a high-pressure turbine cascade". *Journal of Turbulence*, Vol. 11, p. N6.

Carr, L.W. and Chandrasekhara, M., 1996. "Compressibility effects on dynamic stall". *Progress in Aerospace Sciences*, Vol. 32, No. 6, pp. 523–573. ISSN 0376-0421. doi:https://doi.org/10.1016/0376-0421(95)00009-7. URL https://www.sciencedirect.com/science/article/pii/0376042195000097.

Corke, T.C. and Thomas, F.O., 2015. "Dynamic stall in pitching airfoils: aerodynamic damping and compressibility effects". *Annual Review of Fluid Mechanics*, Vol. 47, pp. 479–505.

Firdaus, R., Kiwata, T., Kono, T. and Nagao, K., 2015. "Numerical and experimental studies of a small vertical-axis wind turbine with variable-pitch straight blades". *Journal of Fluid Science and Technology*, Vol. 10, No. 1, pp. JFST0001–JFST0001.

Franchina, N., Kouaissah, O., Persico, G. and Savini, M., 2022. "Three-dimensional modeling and investigation of the flow around a troposkein vertical axis wind turbine at different operating conditions". *Renewable Energy*, Vol. 199, pp. 368–381.

Fujisawa, N. and Shibuya, S., 2001. "Observations of dynamic stall on darrieus wind turbine blades". *Journal of Wind Engineering and Industrial Aerodynamics*, Vol. 89, No. 2, pp. 201–214.

Garmann, D.J. and Visbal, M.R., 2018. "Challenges and perspectives on cfd and experimental interactions for complex unsteady flows". *Journal of Physics: Conference Series*. doi:10.2514/6.2018-3321. URL https://arc.aiaa.org/doi/abs/10.2514/6.2018-3321.

Hao, W., Mao, H., Lyu, S. and Li, C., 2022. "Study on aerodynamic load reduction and efficiency improvement of vawt based on dtef". *Ocean Engineering*, Vol. 260, p. 111966.

Henne, S., Fouest, S.L. and Mulleners, K., 2020. "Dynamic stall on an airfoil undergoing vawt blade angle of attack variations". *Journal of Physics: Conference Series*, Vol. 1618, No. 5, p. 052033. doi:10.1088/1742-6596/1618/5/052033. URL https://dx.doi.org/10.1088/1742-6596/1618/5/052033.

Laneville, A. and Vittecoq, P., 1986. "Dynamic Stall: The Case of the Vertical Axis Wind Turbine". *Journal of Solar Energy Engineering*, Vol. 108, No. 2, pp. 140–145. ISSN 0199-6231. doi:10.1115/1.3268081. URL https://doi.org/10.1115/1.3268081.

Le Fouest, S. and Mulleners, K., 2022. "The dynamic stall dilemma for vertical-axis wind turbines". *Renewable Energy*, Vol. 198, pp. 505–520.

Liu, Q., Miao, W., Bashir, M., Xu, Z., Yu, N., Luo, S. and Li, C., 2022. "Aerodynamic and aeroacoustic performance assessment of a vertical axis wind turbine by synergistic effect of blowing and suction". *Energy Conversion and Management*, Vol. 271, p. 116289.

Lui, H.F. and Wolf, W.R., 2019. "Construction of reduced-order models for fluid flows using deep feedforward neural networks". *Journal of Fluid Mechanics*, Vol. 872, pp. 963–994.

McCroskey, W.J., 1981. "The phenomenon of dynamic stall". Technical report.

Miotto, R.F., Wolf, W.R., Gaitonde, D. and Visbal, M., 2022a. "Analysis of the onset and evolution of dynamic stall vortex on a periodic plunging airfoil". *Journal of Fluid Mechanics*, Vol. 938, pp. A24.1–A24.29. doi:10.1017/jfm.2022.165.

Miotto, R., Wolf, W., Gaitonde, D. and Visbal, M., 2022b. "Analysis of the onset and evolution of a dynamic stall vortex on a periodic plunging aerofoil". *Journal of Fluid Mechanics*, Vol. 938.

Miotto, R.F., Wolf, W., Gaitonde, D. and Visbal, M.R., 2021. "Pitch-plunge equivalence in dynamic stall of ramp motion airfoils". In *AIAA AVIATION 2021 FORUM*. p. 2519.

Nagarajan, S., Lele, S.K. and Ferziger, J.H., 2003. "A robust high-order compact method for large eddy simulation". *Journal of Computational Physics*, Vol. 191, No. 2, pp. 392–419. ISSN 0021-9991.

Ramos, B.L.O., Wolf, W.R., Yeh, C.A. and Taira, K., 2019a. "Active flow control for drag reduction of a plunging airfoil under deep dynamic stall". *Physical Review Fluids*, Vol. 4, p. 074603. doi:10.1103/PhysRevFluids.4.074603.

Ramos, B.L., Wolf, W.R., Yeh, C.A. and Taira, K., 2019b. "Active flow control for drag reduction of a plunging airfoil under deep dynamic stall". *Physical Review Fluids*, Vol. 4, No. 7, p. 074603.

Simão Ferreira, C., Van Kuik, G., Van Bussel, G. and Scarano, F., 2009. "Visualization by piv of dynamic stall on a vertical axis wind turbine". *Experiments in fluids*, Vol. 46, No. 1, pp. 97–108.

Simão Ferreira, C., Van Zuijlen, A., Bijl, H., Van Bussel, G. and Van Kuik, G., 2010. "Simulating dynamic stall in a two-dimensional vertical-axis wind turbine: verification and validation with particle image velocimetry data". *Wind Energy: An International Journal for Progress and Applications in Wind Power Conversion Technology*, Vol. 13, No. 1, pp. 1–17.

Venkatraman, K., Moreau, S., Christophe, J. and Schram, C.F., ???? "Numerical investigation of the noise radiated by an h-darrieus wind turbine at different tip speed ratios". *28th AIAA/CEAS Aeroacoustics 2022 Conference*. doi:10.2514/6.2022-3058. URL https://arc.aiaa.org/doi/abs/10.2514/6.2022-3058.

Visbal, M.R., 2011. "Numerical investigation of deep dynamic stall of a plunging airfoil". *AIAA Journal*, Vol. 49, No. 10, pp. 2152–2170. doi:10.2514/1.J050892.

Visbal, M.R., ???? *Control of Dynamic Stall on a Pitching Airfoil Using High-Frequency Actuation*. doi:10.2514/6.2015-1267. URL https://arc.aiaa.org/doi/abs/10.2514/6.2015-1267.

Wolf, W.R., Azevedo, J.L.F. and Lele, S.K., 2012. "Convective effects and the role of quadrupole sources for aerofoil aeroacoustics". *Journal of Fluid Mechanics*, Vol. 708, p. 502–538. doi:10.1017/jfm.2012.327.

6. RESPONSIBILITY NOTICE

The authors are the only responsible for the printed material included in this paper.